Robotica (2016) volume 34, pp. 973–994. © Cambridge University Press 2014
doi:10.1017/S0263574714002008

A walking control strategy combining global sensory reflex and leg synchronization

Chenglong Fu†‡*, Jianmei Wang†, Ken Chen†‡, Zhangguo Yu§ and Qiang Huang§

†*State Key Laboratory of Tribology, Tsinghua University, Beijing 100084, China*
‡*Department of Mechanical Engineering, Tsinghua University, Beijing 100084, China*
§*Key Laboratory of Biomimetic Robots and Systems, Beijing Institute of Technology, Beijing 100081, China*

(Accepted June 23, 2014. First published online: July 31, 2014)

SUMMARY
Biped walking can be regarded as a global limit cycle whose stability is difficult to verify by only local sensory feedback. This paper presents a control strategy combining global sensory reflex and leg synchronization. The inverted pendulum angle is utilized as global motion feedback to ensure global stability, and joint synchronization between legs is designed to stabilize bifurcations. The proposed strategy can achieve a stable gait and stabilize bifurcations. The robustness of this approach was evaluated against external disturbances. Walking experiments of a biped actuated by pneumatic muscles were conducted to confirm the validity of the proposed method. Instead of tracking predetermined trajectories, this method uses sensory reflexes to activate motor neurons and coincides with the biological idea wherein inessential degrees-of-freedom are barely controlled rather than strictly controlled.

KEYWORDS: Biped locomotion; Walking control; Global sensory reflex; Leg synchronization.

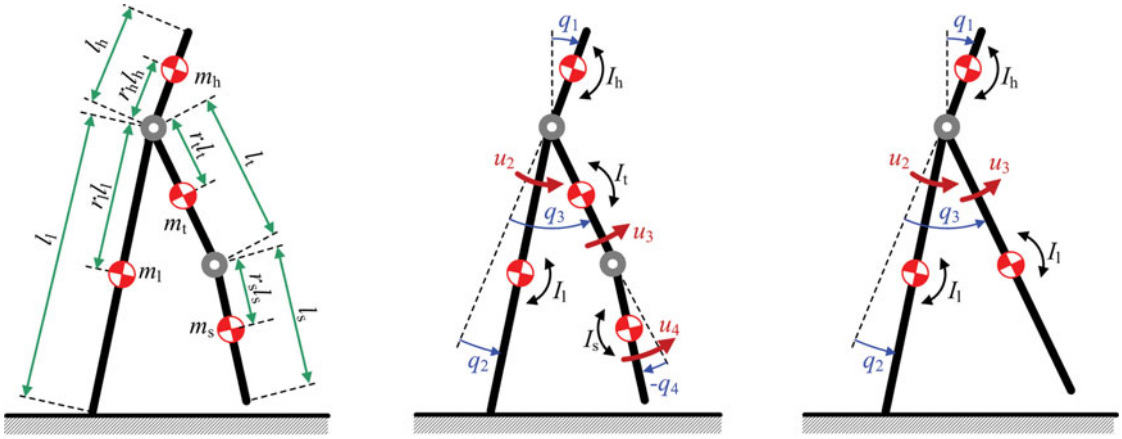
1. Introduction

Trajectory planning is one of the most popular methods to generate biped walking patterns: joint trajectories generated offline and online under various constraint conditions are followed by actuators to realize stable walking.[1,2] To track kinematic trajectories precisely, high-gain position control and extremely accurate ground models are needed. The methodology of this method seems to be opposite to human beings, wherein inessential degrees-of-freedom (DOF) are barely controlled.

Human beings seem not to track joint angles precisely while walking, yet can achieve stable and efficient locomotion. This may benefit from the regulation of neuro–musculo–skeletal system.[3] Researchers have proposed some biomimetic control methods inspired by this phenomenon. One is a CPG-based approach,[4] which produces self-sustained rhythm signals by neural network assisting when necessary with the modulation of the central pattern generator (CPG) to proprioceptive information through sensory inputs.[5,6] The disadvantage of this approach is that the number of network parameters is relatively large; therefore it is difficult to shape output signals and establish a correlation between control parameters and walking performances.[7] Another is a reflex-based approach, which activates motor neurons by sensory input directly.[8] Many attempts have been made to utilize this approach to control multi-leg robots;[9,10] however, in the field of biped robots, it is usually used as a supplement.[11–13] It is difficult to achieve global stability only depending on local reflexes since static instability during swing phase makes the biped robot tend to tumble. There are only a few studies on the control of biped walking by reflexes. Geng *et al.*[14] design a pure sensor-driven controller and apply it on a planar biped robot successfully. It is the first time that fast biped walking is achieved only by reflexes. Manoonpong *et al.*[15] present an adaptive reflex strategy by including

* Corresponding author. E-mail: fcl@tsinghua.edu.cn

https://doi.org/10.1017/S0263574714002008 Published online by Cambridge University Press



(a) Link parameters (b) Coordinates for 4-DOF model (c) Coordinates for 3-DOF model

Fig. 1. Link parameters and coordinate definition of biped robot.

online learning mechanisms based on simulated synaptic plasticity, and make a small biped robot learn to adapt to changes in the terrain to a certain degree.

Although many bio-inspired control methods have been proposed to realize stable walking successfully, at least two problems still remain unsolved. First, global feedback signals have not been utilized while designing the sensory feedback network. Grizzle *et al.*[16] and Westervelt *et al.*[17] demonstrate that asymptotically stable walking can be achieved by making all actuated joints track the predetermined functions of the absolute angle of inverted pendulum. Although this may be somewhat opposite to biological unconstrained idea, we believe that the global walking information plays an important role in enhancing also the robustness of bipedal walking for bio-inspired control strategies. Second, gait bifurcations tend to occur while using the force control strategy,[7] which may be partly due to the fact that the motion between support leg and swing leg cannot be coordinated synchronously.

In this paper, we present a walking rhythm controller for a kneed biped robot with torso based on biological inspiration. The controller consists of global motion feedback for periodic motion, leg synchronization feedback for stabilization of generated gaits, and joint angle feedback for mimicking human muscle behavior. The proposed method can achieve a stable gait and stabilize bifurcations. The robustness of this method was evaluated against external disturbances. Experiments were conducted to confirm the validity of the proposed method. Instead of tracking predetermined trajectories, we use sensory reflexes to activate motor neurons, and this coincides with the biological idea wherein inessential DOFs are barely controlled rather than strictly controlled.

The rest of this paper is organized as follows. Section 2 describes a kneed biped model and introduces the analytical model. Section 3 describes the proposed walking strategy. Section 4 shows the simulation results of typical steady locomotion, including robustness against control parameters and external disturbance, and discusses the effects of parameters on walking performance. Section 5 introduces a planar biped actuated by pneumatic muscles, and conducts walking experiments to confirm the robustness of control strategy. Finally, in Section 6 we conclude the paper.

2. Model of Kneed Biped Robot

2.1. Biped mechanism and basic hypotheses

The biped robot considered in this paper consists of a torso and two legs. Each leg comprises a thigh and a shank connected at a knee joint. There is no actuation at the stance leg tip. Hence, the robot is underactuated. Touch sensors are placed on the feet to synchronize biped controller with robot dynamics.

Figure 1 shows link parameters and definition of coordinates, where l_i denotes the link length, r_i denotes the percentage of the mass center, m_i denotes the link mass, and I_i denotes the inertia around the mass center. Link parameters of the robot are shown in Table I.

https://doi.org/10.1017/S0263574714002008 Published online by Cambridge University Press

Table I. Parameter values of a biped robot.

Model parameters	Unit	Link	Label	Value
Mass	kg	Torso	m_{h}	2.0
		Thigh	m_{t}	0.6
		Shank	m_{s}	0.6
		Leg	m_l	1.2
Length	m	Torso	l_{h}	0.15
		Thigh	l_{t}	0.32
		Shank	l_{s}	0.32
		Leg	l_l	0.64
Inertia at mass center	m^2 kg	Torso	I_{h}	0.007
		Thigh	I_{t}	0.005
		Shank	I_{s}	0.005
		Leg	I_l	0.040
Percentage of mass center	%	Torso	r_{h}	15
		Thigh	r_{t}	50
		Shank	r_{s}	50
		Leg	r_l	50

The hypotheses assumed for the desired walking gaits are now enumerated[18,19]:

H1. Walking consists of a single support phase and an instantaneous double support phase.
H2. The support leg is always straight during walking.
H3. The swing leg is fully extended before the moment of ground collision.
H4. Both knee collision and ground collision are assumed to be completely inelastic.

Under the above hypotheses, the single support phase can be divided into two distinct phases from the aspect of DOF. As shown in Fig. 2, the 4-DOF phase starts from the "toe-off" event and ends up with knee collision; and the 3-DOF phase starts from knee collision and ends up with ground collision.

2.2. Motion equations for 4- and 3-DOF phases

The generalized coordinates for 4-DOF phase are defined as $\boldsymbol{q} = (q_1, q_2, q_3, q_4)'$, as shown in Fig. 1(b). The equation of motion for this phase can be written as

$$\begin{bmatrix} D4_{11} & D4_{12} & D4_{13} & D4_{14} \\ & D4_{22} & D4_{23} & D4_{24} \\ & & D4_{33} & D4_{34} \\ \text{sym} & & & D4_{44} \end{bmatrix} \begin{bmatrix} \ddot{q}_1 \\ \ddot{q}_2 \\ \ddot{q}_3 \\ \ddot{q}_4 \end{bmatrix} + \begin{bmatrix} C4_{11} & C4_{12} & C4_{13} & C4_{14} \\ C4_{21} & 0 & C4_{23} & C4_{24} \\ C4_{31} & C4_{32} & C4_{33} & C4_{34} \\ C4_{41} & C4_{42} & C4_{43} & 0 \end{bmatrix} \begin{bmatrix} \dot{q}_1 \\ \dot{q}_2 \\ \dot{q}_3 \\ \dot{q}_4 \end{bmatrix} + \begin{bmatrix} G4_1 \\ G4_2 \\ G4_3 \\ G4_3 \end{bmatrix} = \begin{bmatrix} 0 \\ u_2 \\ u_3 \\ u_4 \end{bmatrix}, \quad (1)$$

where elements $D4_{ij}$, $C4_{ij}$, and $G4_i$ of matrices are shown in Appendix A; u_2, u_3, and u_4 are the torques applied at hip and knee actuators, as shown in Fig. 1(b).

As shown in Fig. 1(c), the generalized coordinates for 3-DOF phase are defined as $(q_1, q_2, q_3)'$. Thus, the equation of motion for this phase becomes

$$\begin{bmatrix} D3_{11} & D3_{12} & D3_{13} \\ & D3_{22} & D3_{23} \\ \text{sym} & & D3_{33} \end{bmatrix} \begin{bmatrix} \ddot{q}_1 \\ \ddot{q}_2 \\ \ddot{q}_3 \end{bmatrix} + \begin{bmatrix} C3_{11} & C3_{12} & C3_{13} \\ C3_{21} & 0 & C3_{23} \\ C3_{31} & C3_{32} & 0 \end{bmatrix} \begin{bmatrix} \dot{q}_1 \\ \dot{q}_2 \\ \dot{q}_3 \end{bmatrix} + \begin{bmatrix} G3_1 \\ G3_2 \\ G3_3 \end{bmatrix} = \begin{bmatrix} 0 \\ u_2 \\ u_3 \end{bmatrix}, \quad (2)$$

where elements $D3_{ij}$, $C3_{ij}$, and $G3_i$ of matrices are shown in Appendix B.

2.3. Equations governing knee collision and ground collision

Let $\boldsymbol{q}^-$, $\boldsymbol{q}^+$, $\dot{\boldsymbol{q}}^-$, and $\dot{\boldsymbol{q}}^+$ denote the pre- and post-impact generalized positions and generalized velocities respectively. Superscripts "–" and "+" denote quantities immediately before and after impact in the following part of this paper.

https://doi.org/10.1017/S0263574714002008 Published online by Cambridge University Press

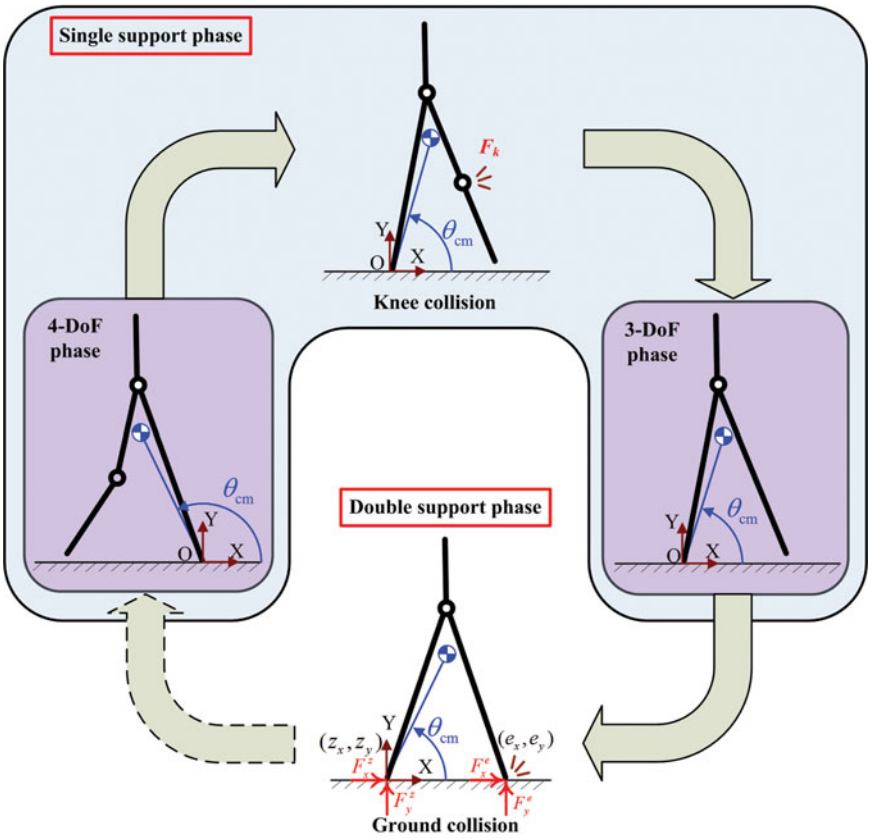


Fig. 2. Phases of biped locomotion.

Knee collision occurs when the shank comes in line with the thigh. Under hypothesis H4, Eq. (1) is "integrated" over the "duration" of the collision to obtain[20]

$$\boldsymbol{D4}(\boldsymbol{q}^+)\dot{\boldsymbol{q}}^+ - \boldsymbol{D4}(\boldsymbol{q}^-)\dot{\boldsymbol{q}}^- = \begin{bmatrix} 0 \\ 0 \\ 0 \\ -\hat{F}_{\mathrm{k}} \end{bmatrix}, \tag{3}$$

where $\hat{F}_{\mathrm{k}}$ is the integral of torque acting on the shank during knee collision. After the collision, the angular velocities of the shank and the thigh become the same, and therefore

$$[0 \quad 0 \quad -1 \quad 1]\dot{\boldsymbol{q}}^+ = 0. \tag{4}$$

Solving Eqs. (3) and (4) yields

$$\begin{bmatrix} \dot{\boldsymbol{q}}^+ \\ \hat{F}_{\mathrm{k}} \end{bmatrix} = \begin{bmatrix} \boldsymbol{D4}(\boldsymbol{q}^+) & \begin{bmatrix} 0 \\ 0 \\ 0 \\ 1 \end{bmatrix} \\ \begin{bmatrix} 0 & 0 & -1 & 1 \end{bmatrix} & 0 \end{bmatrix}^{-1} \begin{bmatrix} \boldsymbol{D4}(\boldsymbol{q}^-)\dot{\boldsymbol{q}}^- \\ 0 \end{bmatrix}. \tag{5}$$

Ground collision occurs when the swing foot touches the ground. The contact model of ground collision requires 5 DOFs of robot.[13] By adding the Cartesian coordinates $(z_x, z_y)'$ to the end of the stance leg, as indicated in Fig. 2, the following extended model is easily obtained through the method

https://doi.org/10.1017/S0263574714002008 Published online by Cambridge University Press

of Lagrange,

$$\boldsymbol{D}_{\mathrm{f}}(\boldsymbol{q}_{\mathrm{f}})\ddot{\boldsymbol{q}}_{\mathrm{f}} + \boldsymbol{C}_{\mathrm{f}}(\boldsymbol{q}_{\mathrm{f}}, \dot{\boldsymbol{q}}_{\mathrm{f}})\dot{\boldsymbol{q}}_{\mathrm{f}} + \boldsymbol{G}_{\mathrm{f}}(\boldsymbol{q}_{\mathrm{f}}) = \boldsymbol{B}_{\mathrm{f}}\boldsymbol{u} + \left(\frac{\partial \boldsymbol{Z}(\boldsymbol{q}_{\mathrm{f}})}{\partial \boldsymbol{q}_{\mathrm{f}}}\right)' \boldsymbol{F}^{z} + \left(\frac{\partial \boldsymbol{E}(\boldsymbol{q}_{\mathrm{f}})}{\partial \boldsymbol{q}_{\mathrm{f}}}\right)' \boldsymbol{F}^{e}, \tag{6}$$

where $\boldsymbol{q}_{\mathrm{f}} = [q_1, q_2, q_3, z_x, z_y]'$ is the set of generalized coordinates, $\boldsymbol{F}^{z} = [F_x^z, F_y^z]'$ and $\boldsymbol{F}^{e} = [F_x^e, F_y^e]'$ are the forces acting on the support leg tip and the swing leg tip at touchdown respectively, $\boldsymbol{Z}(\boldsymbol{q}_{\mathrm{f}}) = [z_x(\boldsymbol{q}_{\mathrm{f}}), z_y(\boldsymbol{q}_{\mathrm{f}})]'$ and $\boldsymbol{E}(\boldsymbol{q}_{\mathrm{f}}) = [e_x(\boldsymbol{q}_{\mathrm{f}}), e_y(\boldsymbol{q}_{\mathrm{f}})]'$ are the Cartesian coordinates of the forward leg tip and the backward leg tip respectively, as shown in Fig. 2. Elements of $\boldsymbol{D}_{\mathrm{f}}(\boldsymbol{q}_{\mathrm{f}})$ and $\boldsymbol{E}(\boldsymbol{q}_{\mathrm{f}})$ are shown in Appendix C.

Collision equation can be obtained through integration of Eq. (6) for the infinitesimal impact time. The ground reaction applied on the swing leg can be considered as an impulsive force at the instant of collision and defined by $\hat{\boldsymbol{F}}^{e} = \int_{t^-}^{t^+} \boldsymbol{F}^{e}(\tau)\mathrm{d}\tau$. It is assumed that the stance leg lifts from the ground without interaction (no friction, no sticking) after the collision;[18] therefore the ground reaction applied on the stance leg tip, $\hat{\boldsymbol{F}}^{z} = \int_{t^-}^{t^+} \boldsymbol{F}^{z}(\tau)\mathrm{d}\tau$, should be null for the infinitesimal impact time. Actuators cannot generate impulses and hence can be ignored during the collsion. Coriolis and gravity forces have finite values, thus they do not influence the collision. Given these conditions, the impact equations can be written in the following form:

$$\boldsymbol{D}_{\mathrm{f}}(\boldsymbol{q}_{\mathrm{f}}^{+}) \cdot \dot{\boldsymbol{q}}_{\mathrm{f}}^{+} - \boldsymbol{D}_{\mathrm{f}}(\boldsymbol{q}_{\mathrm{f}}^{-}) \cdot \dot{\boldsymbol{q}}_{\mathrm{f}}^{-} = \left(\frac{\partial \boldsymbol{E}(\boldsymbol{q}_{\mathrm{f}})}{\partial \boldsymbol{q}_{\mathrm{f}}}\right)' \hat{\boldsymbol{F}}^{e}. \tag{7}$$

Under hypothesis H4, the collision of the swing leg with the ground results in no rebound, and therefore we obtain

$$\left.\frac{\partial \boldsymbol{E}(\boldsymbol{q}_{\mathrm{f}})}{\partial \boldsymbol{q}_{\mathrm{f}}}\right|_{\boldsymbol{q}_{\mathrm{f}}=\boldsymbol{q}_{\mathrm{f}}^{-}} \cdot \dot{\boldsymbol{q}}_{\mathrm{f}}^{+} = 0. \tag{8}$$

Solving Eqs. (7) and (8) yields

$$\begin{bmatrix} \dot{\boldsymbol{q}}_{\mathrm{f}}^{+} \\ \begin{bmatrix} \hat{F}_x \\ \hat{F}_y \end{bmatrix} \end{bmatrix} = \begin{bmatrix} \boldsymbol{D}_{\mathrm{f}}(\boldsymbol{q}_{\mathrm{f}}^{-}) & -\left(\left.\frac{\partial \boldsymbol{E}(\boldsymbol{q}_{\mathrm{f}})}{\partial \boldsymbol{q}_{\mathrm{f}}}\right|_{\boldsymbol{q}_{\mathrm{f}}=\boldsymbol{q}_{\mathrm{f}}^{-}}\right)' \\ \left.\left(\frac{\partial E(\boldsymbol{q}_{\mathrm{f}})}{\partial \boldsymbol{q}_{\mathrm{f}}}\right)\right|_{\boldsymbol{q}_{\mathrm{f}}=\boldsymbol{q}_{\mathrm{f}}^{-}} & \begin{bmatrix} 0 & 0 \\ 0 & 0 \end{bmatrix} \end{bmatrix}^{-1} \begin{bmatrix} \boldsymbol{D}_{\mathrm{f}}(\boldsymbol{q}_{\mathrm{f}}^{-}) \cdot \dot{\boldsymbol{q}}_{\mathrm{f}}^{-} \\ \begin{bmatrix} 0 \\ 0 \end{bmatrix} \end{bmatrix}. \tag{9}$$

3. Walking Strategy

3.1. Overall control strategy

Figure 3 shows the overall block diagram of control strategy combining sensory reflex and leg synchronization. Under hypotheses H2 and H4, we assume that the knee joint is controlled by a locking mechanism (latch) during walking.[21–23] The latch is released swing passively when the foot touch sensor detects the "toe-off" event, and is locked to prepare for the straight leg landing when the shank comes in line with the thigh.[24] Since the swing knee joint is passive, u_4 is set to zero in this paper.

For the hip joint, we introduce the global motion, leg synchronization, and joint angle as sensory feedback to activate motor neurons. One of the basic aspects of biped locomotion is to keep the torso upright. There is no waist joint in our model, and therefore the only way to tune the torso attitude is to control hip joints. Since the dynamic motion of the support leg is not easy to be influenced, we add the torso attitude control into the support hip joint.

https://doi.org/10.1017/S0263574714002008 Published online by Cambridge University Press

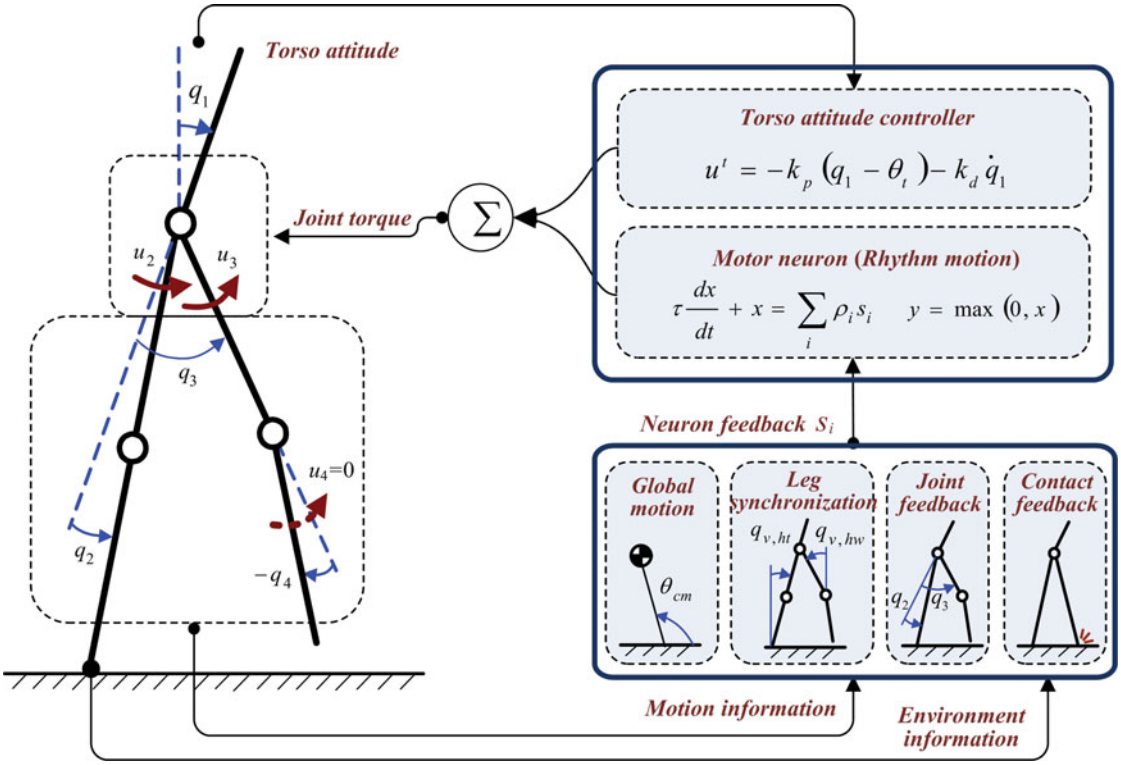


Fig. 3. Overall control block diagram of walking control strategy.

The hip joint torque is designed as

$$\left.\begin{array}{l} u_2 = u_2^r + u^t \\ u_3 = u_3^r \end{array}\right\}, \tag{10}$$

where u_2^r and u_3^r are the rhythm torques of the support hip joint and the swing hip joint respectively, and u^t is the torso attitude torque.

3.2. Rhythm motion controller

3.2.1. Model of motor neurons. Single motor neuron represents a direct connection between the nervous system and the muscles, and it carries signals from the spinal cord to activate the muscles to produce movement. The model of motor neurons is a mathematical description and prediction of biological processes of motor neurons. Among various continuous-variable models representing a single motor neuron's activity, we shall adopt the following widely used model for its mathematical simplicity[4,14]:

$$\left.\begin{array}{l} \tau\frac{\mathrm{d}x}{\mathrm{d}t} + x = \sum_i \rho_i S_i \\ y = \max(0, x) \end{array}\right\}, \tag{11}$$

where x represents the mean membrane potential of the motor neuron, y is the output of the motor neuron, ρ_i represents the strength of the sensory synaptic conjunction, S_i is sensory feedback signal, and τ is a time constant associated with the passive properties of cell membrane.

The rotation of each joint is controlled by two motor neurons corresponding to extensor and flexor muscles, and the rhythm joint torque u_i is designed as

$$u_i^r = g_i \cdot (y_{ei} - y_{fi}), \tag{12}$$

https://doi.org/10.1017/S0263574714002008 Published online by Cambridge University Press

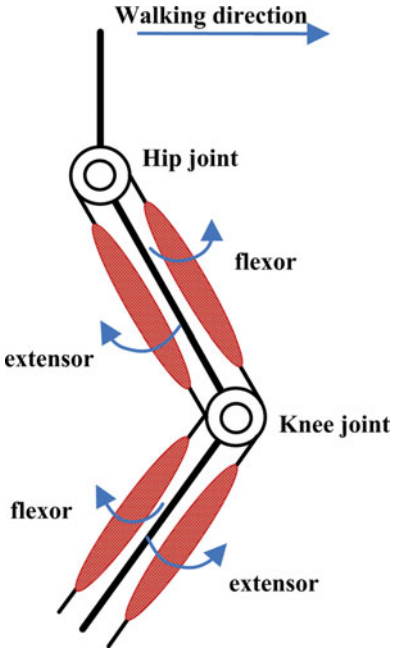


Fig. 4. Directions of extensor movements and flexor movements.

where y_{ei} and y_{fi} are outputs of extensor neuron and flexor neuron respectively, and g_i is the gain of out torque. The directions of extensor and flexor movements are defined according to the anatomy shown in Fig. 4.

One of the main characters of biomimetic control based on reflexes is that the output of motor neuron depends on sensory feedback S_i, instead of mutual inhibition between neurons; therefore, the design of S_i is essential for rhythm generation.

3.2.2. Global motion feedback. Legged locomotion can be described from two points of view: one is in joint space, and another is in task space. Although biped robots are typically high DOF mechanisms, the task of biped locomotion is inherently a low-DOF task.[17] Considering planar walking, the task is to achieve the movement of center of mass (COM) of biped robot in sagittal plane. We simplify the task space to be an inverted pendulum and let θ_{cm} denote the absolute angle of the pendulum, as shown in Fig. 2. In normal walking, θ_{cm} is a monotonic quantity which can represent the evolution state of periodical walking.

Stable and flexible biped locomotion depends on a global entrainment between the controller, the biped robot, and the environment,[5,14] that is, the control torque of each joint, states of the biped robot, and the interaction with the environment must maintain a consistent rhythm. This requires the control torque to keep pace with robot's periodic motion. Grizzle *et al.*[16] and Westervelt *et al.*[17] demonstrated that the synchronization between the absolute angle of inverted pendulum and the actuated joints could achieve asymptotically stable walking.[16,17] Inspired by this work, we introduce a global motion feedback S_{cm} as

$$S_{\text{cm}} = \frac{1}{1 + \exp(-\alpha_{\text{cm}}(\theta_{\text{cm}} - \Theta_{\text{cm}}))}, \tag{13}$$

where θ_{cm} is the absolute angle of inverted pendulum, as shown in Fig. 2, Θ_{cm} is the threshold, and α_{cm} is a positive constant. Fig. 5(a) demonstrates S_{cm} with respect to θ_{cm} with different values of Θ_{cm}. From Fig. 5(a), one can see that a large value of the threshold Θ_{cm} will result in a rightward shift of the curve of S_{cm} with respect to θ_{cm} without changing the slope curve. In normal forward walking, θ_{cm} decreases monotonically during a step; therefore, the global motion feedback S_{cm} also decreases monotonically versus time within a step. The reason for this design is that for underactuated biped robots, more energy should be injected in the initial stage than in the latter stage to overcome the effect of gravity. A larger value of the threshold results in the decrement of S_{cm}. Fig. 5(b) demonstrates S_{cm}

https://doi.org/10.1017/S0263574714002008 Published online by Cambridge University Press

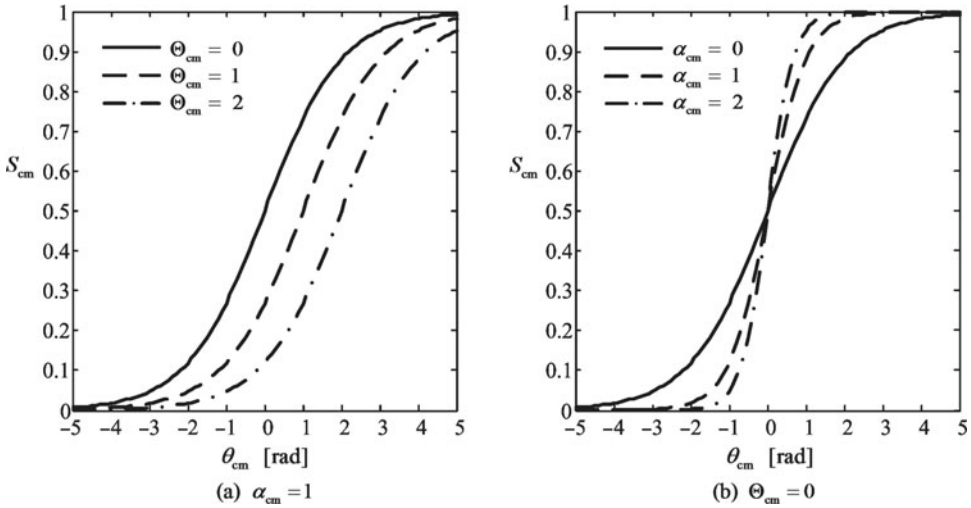


Fig. 5. Global motion feedback S_{cm} versus θ_{cm} with different values of Θ_{cm} and α_{cm}.

with respect to θ_{cm} with different values of α_{cm}. From Fig. 5(b), one can see that a larger α_{cm} value means a steeper increase of S_{cm} relative to θ_{cm}. This model is inspired by a sensor neuron model presented by Geng *et al.*[14] and Wadden *et al.*,[28] and is thought capable of emulating the response characteristics of populations of sensor neurons in animals.

3.2.3. Leg synchronization feedback. Biomimetic control strategy attempts to imitate the neuro–musculo–skeletal system of human beings, and take the output of motor neuron as a joint control force. This strategy can utilize robot's inherent dynamic property; however, comparing with the trajectory tracking method, the robot tends to exhibit period doubling and apparently chaotic gait.[7] This phenomenon also occurs in the passive dynamic walking along with increase in slope angle.[25] The study of powered bipeds based on passive dynamic principles indicates that robot will never fall forward if swing and support legs are synchronized appropriately.[26] A good case in point is rimless wheel: Given a suitable initial condition, the rimless wheel rolls down a slope, and the rolling always converges to a period-one stable gait as long as the next collision occurs.[27] Therefore, we conjecture that synchronization between the swing leg and the support leg may help to stabilize bifurcations and chaos.

Let q_{hw} and q_{ht} denote the absolute angles of the swing leg and the support leg respectively, as shown in Fig. 6. At initial and final stages, one can obtain $q_{hw} + q_{ht} = 0$; therefore, we introduce the leg synchronization S_q as

$$S_q = \begin{cases} -(q_{hw} - \theta_q(q_{ht}) - \Theta_q), & q_4 < 0 \\ -(q_{hw} + q_{ht}), & q_4 = 0 \end{cases}, \tag{14}$$

where q_4 is the relative angle of the swing knee joint, and Θ_q is the angle bias which can be used to tune the foot clearance of the swing leg, and θ_q is the virtual absolute angle of the thigh when the shank is vertical and touches the ground, as shown in Fig. 6. θ_q can be calculated according to q_{ht} by

$$\theta_q(q_{ht}) = \arccos\left(\frac{(l_t + l_s)\cos q_{ht} - l_s}{l_t}\right), \tag{15}$$

where l_t and l_s are the length of thigh and shank respectively.

Leg synchronization feedback S_q is connected to motor neurons of the swing-hip joint. The first purpose of its design is to coordinate the swing leg with the support leg approximately symmetrically during walking, especially at initial and final stages. The second purpose is to achieve enough foot clearance in the swing phase during walking.

https://doi.org/10.1017/S0263574714002008 Published online by Cambridge University Press

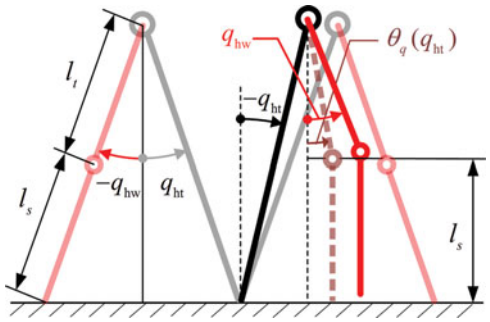


Fig. 6. Geometry constraints of leg synchronization.

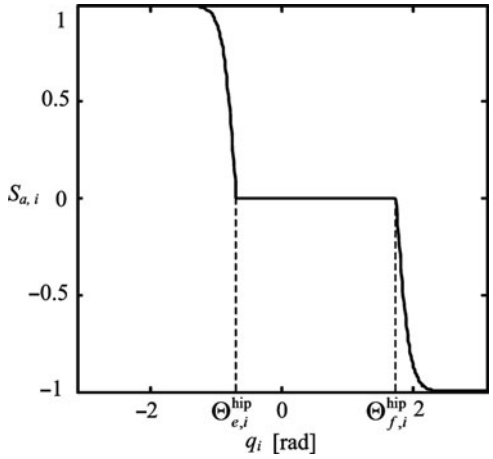


Fig. 7. Joint angle feedback versus joint angle.

3.2.4. Joint angle feedback. Biological investigations suggest that when the joint movement is beyond a certain range, muscles will contract to limit the range of the joint movement and reset the phase of limbs; therefore the joint angle feedback $S_{a,i}$ is designed as

$$S_{a,i} = \begin{cases} \dfrac{1-\exp\left(\alpha_a(q_i-\Theta^{hip}_{f,i})\right)}{1+\exp\left(\alpha_a(q_i-\Theta^{hip}_{f,i})\right)}, & q_i > \Theta^{hip}_{f,i} \\ 0, & \Theta^{hip}_{e,i} < q_i < \Theta^{hip}_{f,i} \\ \dfrac{1-\exp\left(\alpha_a(q_i-\Theta^{hip}_{e,i})\right)}{1+\exp\left(\alpha_a(q_i-\Theta^{hip}_{e,i})\right)}, & q_i < \Theta^{hip}_{e,i} \end{cases}, \tag{16}$$

where $\Theta^{hip}_{f,i}$ and $\Theta^{hip}_{e,i}$ are hip joint's Anterior Extreme Angle (AEA) and Posterior Extreme Angle (PEA) associated with the extreme angles of flexor and extensor respectively, and α_a is a positive constant. A larger α_a value means a steeper increase of $S_{a,i}$ relative to q_i. Figure 7 shows a typical curve of the joint angle feedback $S_{a,i}$ relative to the joint angle q_i.

3.2.5. Reflex network. The network between sensory feedback and motor neurons is shown in Fig. 8, where the connection weights of excitatory synapses are positive, and the connection weights of inhibitory synapses are negative. The global motion feedback S_{cm} has excitatory (inhibitory) connections to the motor neurons of the support hip extensor (flexor) and the swing-hip flexor (extensor), and this design can conduce to rotate the support hip joint backward and rotate the swing-hip joint forward during walking. Leg synchronization feedback S_q is only connected to the motor neurons of the swing-hip joint. Since the moment of inertia of the swing leg at the hip is smaller than

https://doi.org/10.1017/S0263574714002008 Published online by Cambridge University Press

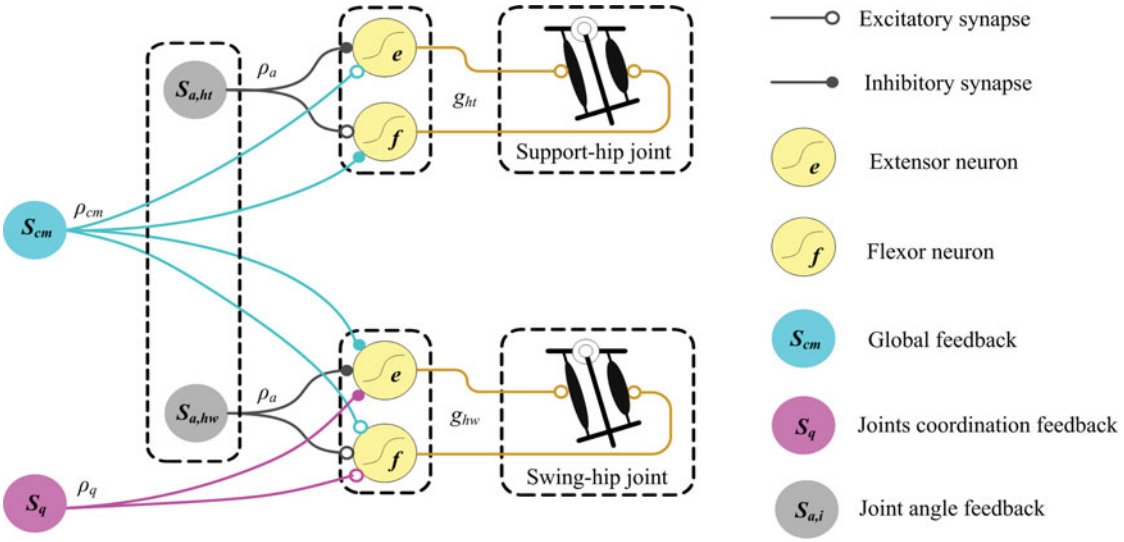


Fig. 8. Sensory reflex network.

that of the support hip, it will take less force to coordinate two legs by tuning the motion of the swing leg. Joint angle feedback $S_{a,i}$ is a local feedback for each joint.

3.3. *Torso attitude controller*

To hold the torso around a desired angle, we add the torso attitude torque u^t into the support hip joint by applying PD control scheme,[16]

$$u^t = -k_p(q_1 - \theta_t) - k_d\dot{q}_1, \tag{17}$$

where q_1 and $\dot{q}_1$ are the absolute angle and velocity of the torso as defined in Fig. 1, θ_t is the desired torso angle, and k_p and k_d are the control gains.

4. Simulation Results and Characteristics of Walking

4.1. *Typical features of steady biped locomotion*

We constructed the biped robot model in the simulation environment of Mathworks MATLAB/Simulink. Control parameters of the reflexive controller are defined in Table II. The criterion to choose these parameters is summarized as follows. The time constant τ of the motor neuron determines the response speed of neurons with sensory input and it is set as 0.01 s to respond to the feedback quickly. α_a and α_{cm}, which influence the steepness of sensory feedback relative to motion angles, can be selected according to the desired range of joint angle q_i and the inverted pendulum angle θ_{cm}. Joint extreme angles $\Theta^{\mathrm{hip}}_{f,i}$ and $\Theta^{\mathrm{hip}}_{e,i}$ can be determined according to the human motion range data. The threshold of the global motion feedback Θ_{cm} reflects the middle angle of the global motion feedback. To inject more energy in the initial stage than the latter stage, Θ_{cm} was selected to be greater than $\pi/2$ to overcome the potential energy barrier. The bias angle Θ_q, used to tune foot clearance during walking, was set as a small value for level walking. The weight value of ρ_a can be determined by the amplitude of the desired limit torque. Connection weights ρ_{cm} and ρ_q can be selected from a stability region, which will be discussed in Section 4.2. The desired torso angle θ_t has a marked effect on the desired walking speed and it can be selected from a wide range.

Since the biped walking corresponds to a limit cycle in the state space, the robot must start from initial conditions within the basin of the limit cycle. We used a simplified inverted pendulum to estimate initial conditions that lead to a stable limit cycle, as shown in Fig. 2. Let L denote the length from the COM to the pivot point, I denote the inertia about the pivot point, and M denote the total mass. According to the angular momentum balance theorem,[17] the motion equation can be

https://doi.org/10.1017/S0263574714002008 Published online by Cambridge University Press

Table II. Control parameters.

τ	g_i	$\alpha_{\rm cm}$	$\Theta_{\rm cm}$	$\rho_{\rm cm}$	Θ_q	ρ_q	α_a	$\Theta_{f,i}^{\rm hip}$	$\Theta_{e,i}^{\rm hip}$	ρ_a	θ_t	k_p	k_d
0.01	1.0	20	1.71	1.5	0.02	0.5	30	1.75	−0.7	1.0	0.175	1.0	0.5

written as $I\ddot{\theta}_{\rm cm} + MgL\cos(\theta_{\rm cm}) = 0$. By linearization of this equation at $\theta_{\rm cm} = \pi/2$, we can obtain the analytical solution as

$$\theta_{\rm cm} = \frac{\pi}{2} - \frac{\Phi_0}{\sin(\lambda_0 T/2)}\sin(\lambda_0 t), \tag{18}$$

where Φ_0 is the half stride angle of the pendulum, $\lambda_0 = \sqrt{MgL/I}$, and T is the step period. Differentiating Eq. (18) at $t = T/2$ leads to

$$\frac{\dot{\theta}_{\rm cm}}{\Phi_0} = \frac{\lambda_0}{\tan(\lambda_0 T/2)}, \tag{19}$$

which indicates the ratio of the initial angular velocity and the half stride angle of inverted pendulum. Regardless of the swing amplitude, the step period T has a minor change and varies near 0.65 s (see Fig. 14 in Section 4.3); therefore we fixed the step period for simplification. The robot with the parameter values shown in Table I has a relationship of $\dot{q}_2 = -3.0 \times (q_2 - q_3)$ at the beginning of the swing phase. The joint velocities of the torso and the swing leg should have initial conditions such as $\dot{q}_1 = \dot{q}_3 = \dot{q}_4 = 0$. For initial joint angles at the beginning of the swing phase, the swing knee angle q_4 should be zero, the ground constraint condition can be written as $2q_1 - q_3 - q_2 = 0$, and the initial torso angle q_1, which can be selected from a relative wide range (see Fig. 14 in Section 4.3), is set to 0.2; therefore the initial joint angles depend only on the stride angle $q_2 - q_3$. From the simulation with these initial conditions, we found that the stable walking can be obtained from any initial stride angle between 0.14 rad and 0.26 rad.

Figure 9 plots the generalized coordinates versus the time. We can see that the torso angle q_1 moves forward at the beginning of the step, and this is the result of ground collision as well as deceleration of the hip joint. The torso angle returns to the desired value under the torso attitude controller at the end of the step. Figure 10 portrays the stick figures of walking behavior. It should be noted that for different initial conditions with the same control parameters, the same stable limit cycle is obtained. This indicates that the stable limit cycle is unique for particular control parameters.

Gait bifurcations tend to occur while using torque-based control approach. We design the leg synchronization feedback to stabilize period-two walking. To compare the effect of bifurcation suppression, we conduct a comparative study with our previous delayed feedback control (DFC) method, which adjusted the amplitude and frequency of hip oscillator according to the error of prior step periods.[7] The oscillator is designed as an intermittent sinusoid,

$$u_3(t) = \begin{cases} A \cdot \sin\left[\omega \cdot \left(t - t_{\rm G}^i\right) + \phi_0\right] + B, & t_{\rm G}^i < t \le t_{\rm K}^i \\ 0, & t_{\rm K}^i < t \le t_{\rm G}^{i+1} \end{cases}, \tag{20}$$

where A is the amplitude, ω is the frequency, B is the bias, $t_{\rm G}^i$ and $t_{\rm K}^i$ are the time instants of ground collision and knee collision at the ith step respectively, and ϕ_0 is oscillator initial phase. To stabilize bifurcations, the DFC method adjusts the oscillator as $A^{i+1} = A^i + K_A \cdot (T^i - T^{i-1})$ and $\omega^{i+1} = \omega^i + K_\omega \cdot (t^i - t^{i-1})$, where A^i and ω^i are respectively the amplitude and the frequency of the oscillator at the ith step, K_A and K_ω are the control gains, and T^i is the step period of the ith step. Figure 11 demonstrates the results of comparison between the two methods. Bifurcation controller is activated at and after step 10 for both methods. For the proposed method, weight of leg synchronization ρ_q is set to zero before the 10th step. For the DFC method, the amplitude A and the frequency ω are kept constant before the 10th step, and values of these parameters are selected to have a period-two walking pattern similar to that of the proposed method. The bifurcation control parameters of both proposed method and DFC method are optimized to have the quickest converging

https://doi.org/10.1017/S0263574714002008 Published online by Cambridge University Press

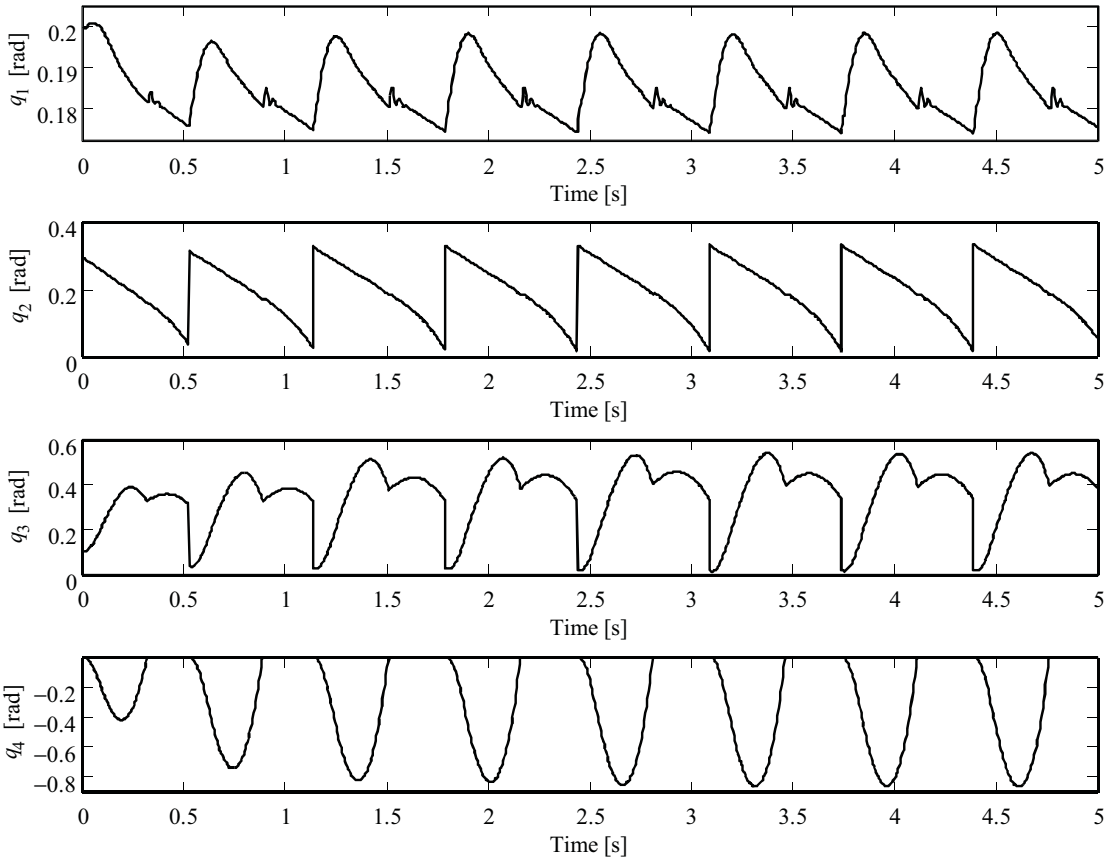


Fig. 9. Joint angles versus time.

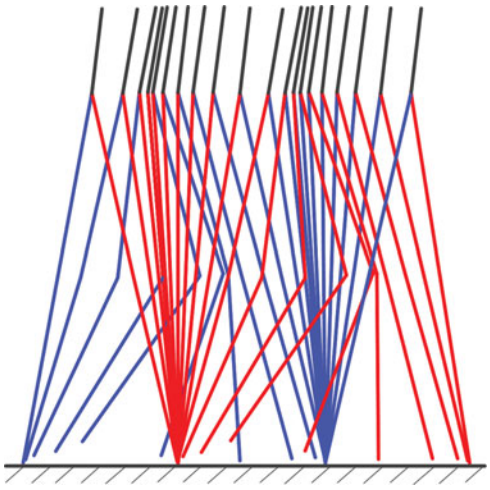


Fig. 10. Stick figures of walking behavior during two steps.

for the given period-two walking. Although there is a slight difference in step periods between the two methods, we can still see that bifurcations can be stabilized more quickly with the proposed method for a given period-two walking.

4.2. Robustness against control parameters and external disturbance

It is interesting to examine the effect of control parameter values on stable walking region. The Poincare method is used to evaluate the stability of walking cycle.[27] The Poincare section is selected

https://doi.org/10.1017/S0263574714002008 Published online by Cambridge University Press

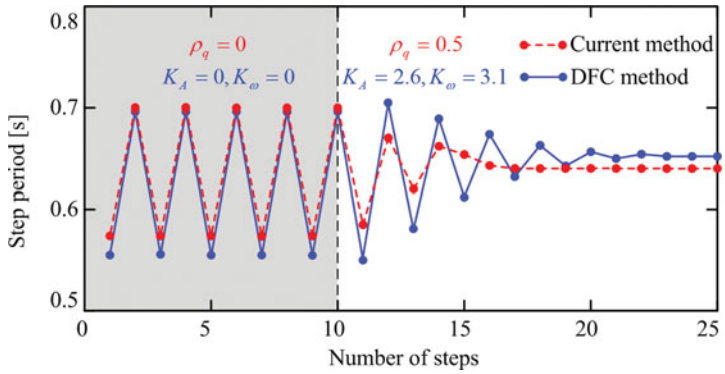
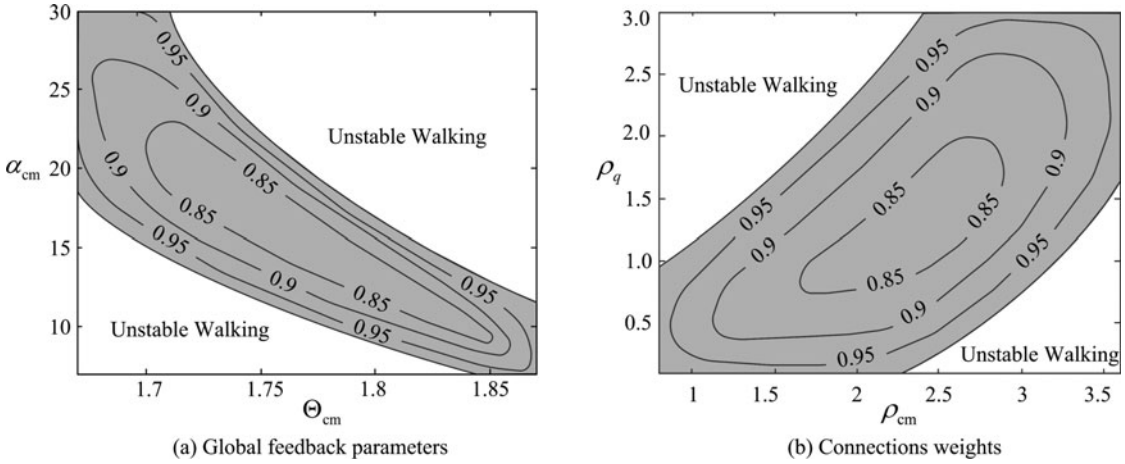


Fig. 11. Comparison of bifurcation control between the current method and the DFC method.



(a) Global feedback parameters (b) Connections weights

Fig. 12. Stability region of control parameters.

as an instance just after heel strike, and the Newton–Raphson methods are used to find the initial condition that was on the limit cycle for the given control parameters. We check cycles' stability by calculating the eigenvalues of the Jacobian of the Poincare map numerically. Figure 12(a) shows the stability region versus global feedback parameters with the same control parameters as given in Table II except for Θ_{cm} and α_{cm}. The shaded areas are the range of global feedback parameters in which stable gaits appear, and the contour is the maximum eigenvalue.

We can see in Fig. 12(a) that a stable walking locomotion can be obtained for a wide range of global feedback parameters with the aforementioned controller. We can also see that increasing threshold Θ_{cm} leads to decreasing α_{cm} to keep walking stable. Figure 12(b) shows the stability region versus connection weights with control parameters in Table II except for ρ_{cm} and ρ_q. We see that for a wide range of connection weights of ρ_{cm} and ρ_q, stable walking can be realized, and this may benefit from the proposed approach, which is designed to keep pace with robot's dynamics during walking. Effect of control parameters on walking performances will be discussed in Section 4.3.

To evaluate the robustness of the proposed control strategy against disturbances, three different pushes were exerted during walking. These pushes are modeled as forces applied to the hip joint for a duration of 0.05 s. The first push is 10 N in magnitude and exerted in a backward direction. The second push is 15 N in magnitude and exerted in a forward direction. The last push is 20 N in magnitude and exerted in a downward direction. In order to allow the controller to act on the whole walking cycle after disturbance, these pushes occur in the beginning of the single support phase. Figure 13(a) demonstrates the stride angle versus time with a backward disturbance; from Fig 13(a), one can see that the stride angle decreases at the collision significantly, which means that the robot slows down due to backward push. However, the stride angle returns to a steady state after several steps. As shown in Figs. 13(b) and (c), the robot can also recover its balance when it is perturbed from

https://doi.org/10.1017/S0263574714002008 Published online by Cambridge University Press

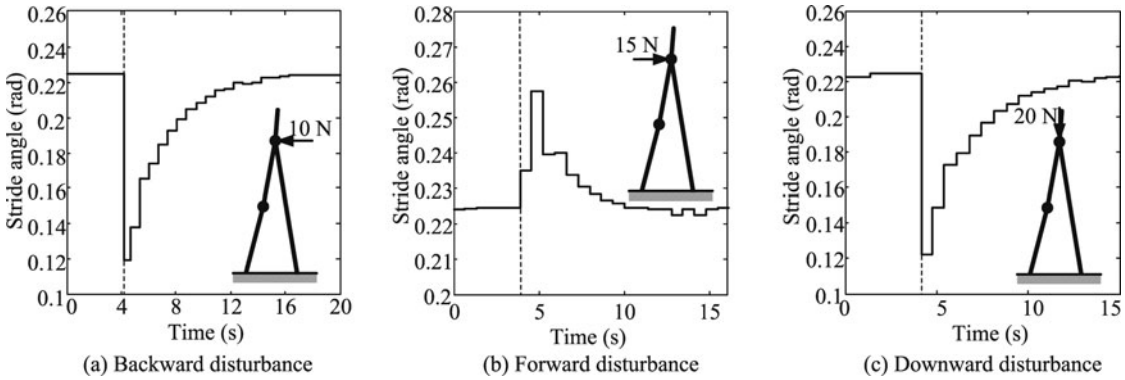


Fig. 13. Results of robustness against external disturbance.

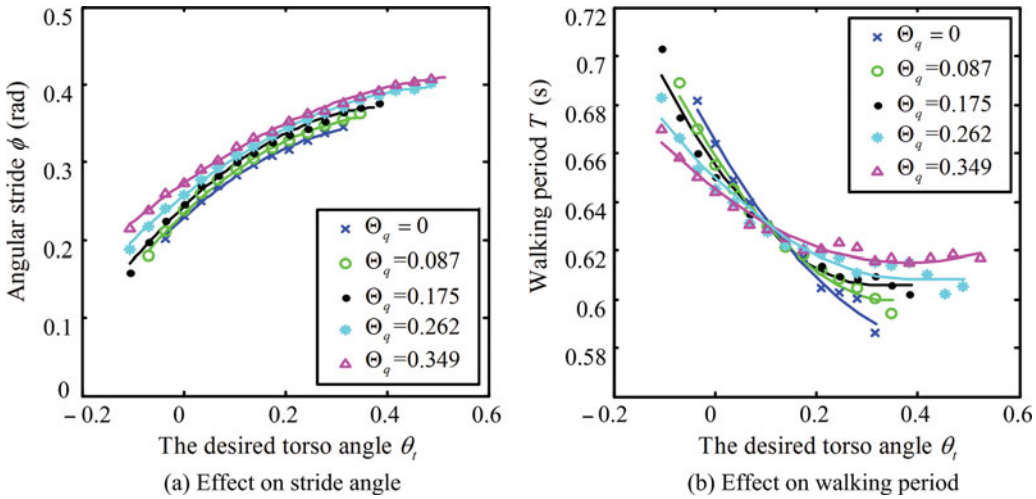


Fig. 14. Effect of the control parameters θ_t and Θ_q on walking indices.

forward and downward directions. It should be noted that the robot can also recover from different start times of the pushes within the stride.

One can see that the stride angle is increasing also in the second step after the forward disturbance in Fig. 13(b). This phenomenon may be explained intuitively as follows. A key feature of dynamic walking is the dissipation of energy at ground collision. When the kinetic energy is larger than nominal, the longer step length can induce larger energy dissipation at collision and the robot may return to periodic orbit over multiple steps. When the robot receives a forward disturbance, the speed is larger than nominal. This induces a shorter step time; therefore, the first step length may be not the longest one. After collision, the speed decreases remarkably and the step time recovers. The step length is also increasing in the second step. This phenomenon is the same as the observation of human motion: one may take two or more steps to recover from a large forward push and choose a relative shorter step length for the first step.

4.3. Effect of parameters

In this section, we will show the effect of control parameters θ_t, Θ_q, ρ_{cm}, and ρ_q on the stride angle and the walking period.

Figures 14(a) and (b) demonstrate the stride angle and the walking period as functions of the desired torso angle θ_t and leg synchronization bias Θ_q respectively. One can see that increasing the desired torso angle θ_t can increase the stride angle and decrease the walking period. In the beginning of the single support phase, robot's COM is behind the support leg tip, and gravity initially decreases the angular momentum of the robot around the support leg tip. After the COM moves past the support leg tip, gravity will increase the angular momentum of the robot. Increasing of θ_t can shift the location

https://doi.org/10.1017/S0263574714002008 Published online by Cambridge University Press

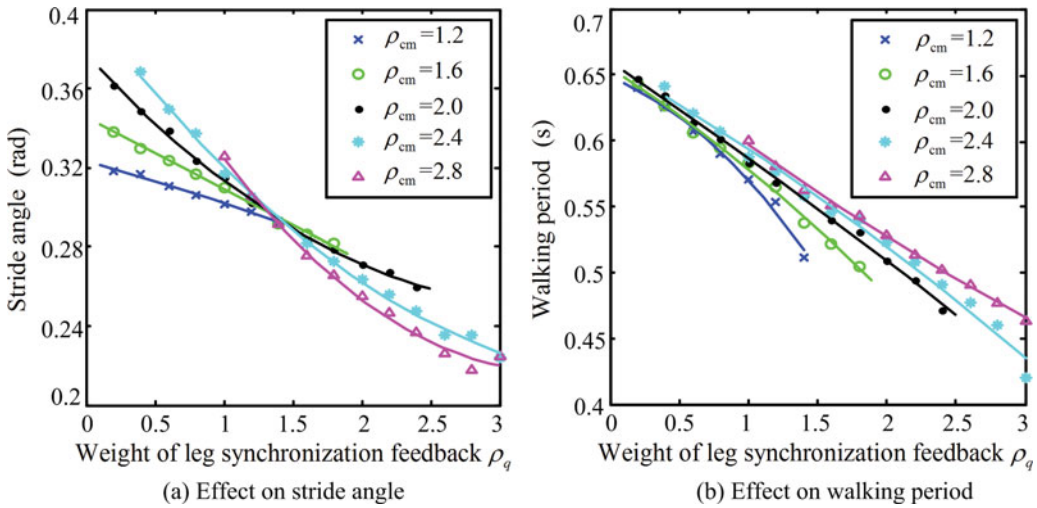


Fig. 15. Effect of the control parameters ρ_{cm} and ρ_q on walking indices.

of the robot's COM forward, and this will shorten the period of deceleration significantly; therefore, θ_t is one of the most effective parameter changes for the regulation of walking speed. The larger the value of Θ_q, the larger the stride angle. There exists a demarcation point of θ_t that before this point, the larger the Θ_q, the smaller the walking period; however, after this point the larger the Θ_q, the larger the walking period.

Weights of global motion feedback ρ_{cm} and leg synchronization feedback ρ_q have effects on the amplitudes of joint torques, and therefore walking performances can also be effected significantly by these two parameters. Figs. 15(a) and (b) show the stride angle and the walking period as functions of the weights of the global motion feedback ρ_{cm} and the leg synchronization feedback ρ_q. One can see that the larger the weight of leg synchronization feedback ρ_q, the smaller the stride angle and the walking period. The larger the weight of global motion feedback ρ_{cm}, the larger the walking period. There exists a demarcation point of ρ_q that before this point, the larger the weight of global motion feedback ρ_{cm}, the larger the stride angle; however, after this point, the larger the weight of global motion feedback ρ_{cm}, the smaller the stride angle.

To enlarge the stride length, the robot can increase the desired torso angle θ_t and the bias angle Θ_q, or decrease the weight of leg synchronization feedback ρ_q. To reduce the stride period, the robot can increase the desired torso angle θ_t and the weight of leg synchronization feedback ρ_q, or decrease the weight of global motion feedback ρ_{cm}. These regulations are limited by the stability region and the maximum joint torques that the robot could provide.

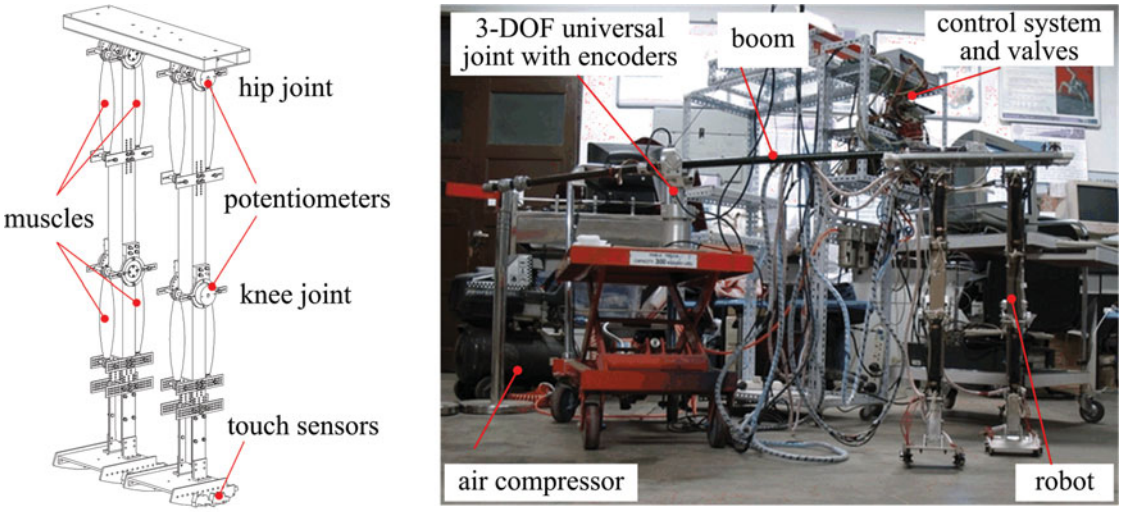
5. Experimental Study

5.1. Experimental biped robot

In order to test the validation of the proposed control strategy, we manufactured the biped robot actuated by antagonistic pneumatic muscles produced by Shadow Robot Company. The length and radius of the muscle are 0.21 m and 0.02 m respectively. As shown in Fig. 16(a), the robot has five links, which are connected by revolute joints. The robot has curved feet in the experiment. Compared with the ideal point feet, the curvature feet can improve walking efficiency. The robot with curve feet touches ground at the heel of the leading leg and at the toe of the trailing leg. This reduces the directional change in COM velocity, and therefore the step-to-step transition work. The curved foot can also allow for long stride lengths because the foot can be extended during ground contact.

In order to constrain walking motions in the frontal plane, the robot was constructed with a radial bar attached at the torso. The bar constrains the sagittal plane to be tangent to a sphere centered at the universal joint, and still allows the robot to freely trip in the sagittal plane. Three encoders are integrated within the universal joint to measure torso's motion, potentiometers are installed at the hip joint and the knee joint to obtain joint angles, and binary contact switches are located at the tip of the

https://doi.org/10.1017/S0263574714002008 Published online by Cambridge University Press



(a) Outline of the robot (b) Experimental setup

Fig. 16. Outline of the robot and the experimental setup.

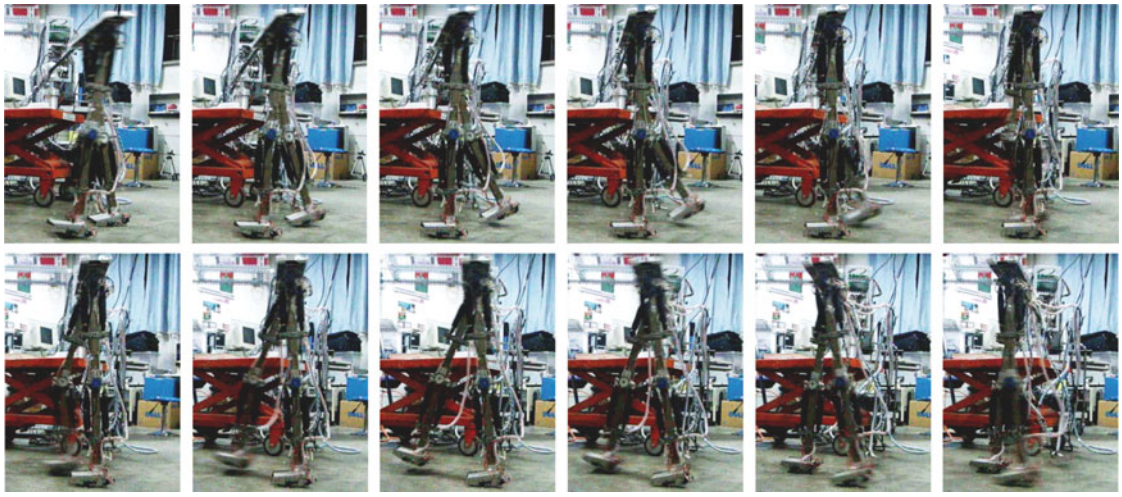


Fig. 17. Frames of normal walking experiment.

leg to detect whether a leg is in contact with the ground. Control system, proportional valves, and air compressor were placed outside the biped, as shown in Fig. 16(b).

5.2. *Experimental results*

First, we demonstrate that the robot can walk on a flat ground with the proposed control strategy. Figure 17 shows the frames of normal walking experiment. The fame interval is 0.09 s, and the average walking stride is about 0.28 m. The average velocity is 0.35 m/s. Figure 18 shows the trajectory of inter-leg angle ϕ versus time; from Fig. 18, one can see that the trajectory of each step is a little bit different. The first reason is that the repeatability of pneumatic muscles is not as good as motors, and the second reason is that the control input is generated according to the walking states of robot instead of tracking planned trajectories.

In order to examine the robustness of the proposed control strategy against unexpected disturbances, a forward push was applied to robot's torso by a person during walking. The push force lasts for about 0.3 s. Figure 19 shows the video frames of the walking experiment with an interval of 0.24 s, and Fig. 20 plots the trajectory of inter-leg angle ϕ versus time. The support leg moves fast after a forward push, and the robot can recover its balance after two short steps.

https://doi.org/10.1017/S0263574714002008 Published online by Cambridge University Press

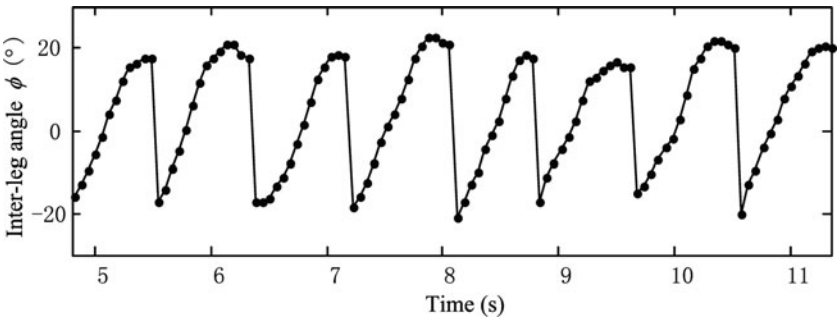


Fig. 18. Inter-leg angle versus time during normal walking.

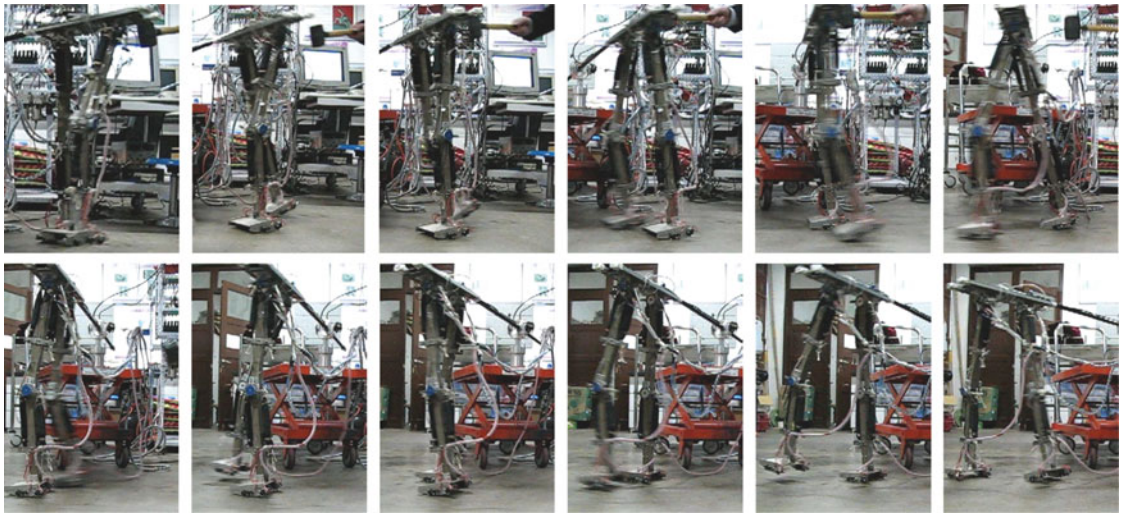


Fig. 19. Frames of walking experiment with forward disturbance.

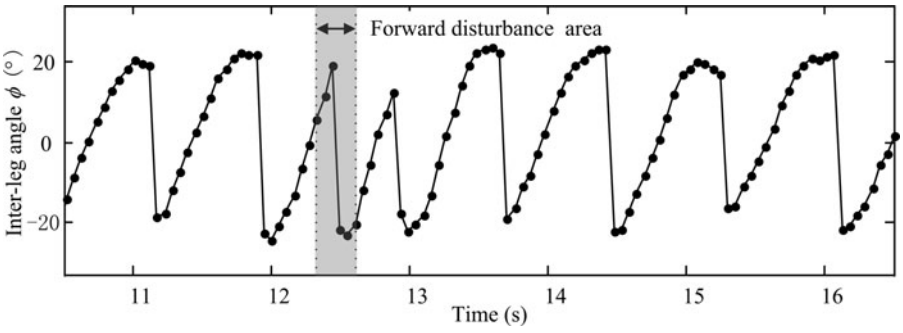


Fig. 20. Inter-leg angle versus time during walking with forward disturbance.

A backward push was also applied to the robot by a person during walking. The push force lasts for about 0.25 s. Figure 21 shows the video frames of the walking experiment with an interval of 0.24 s, and Fig. 22 plots the trajectory of inter-leg angle ϕ versus time. From Figs. 21 and 22, we can see that the robot moves slow after a backward push and can tolerate this disturbance with the proposed strategy.

6. Conclusions and the Future Work

In this paper, we present a walking rhythm control controller combining sensory reflex and leg synchronization. Instead of planning and tracking joint angles precisely, this strategy is inspired by the regulation mechanism of neuro–musculo–skeletal system, and generates walking gait according

https://doi.org/10.1017/S0263574714002008 Published online by Cambridge University Press

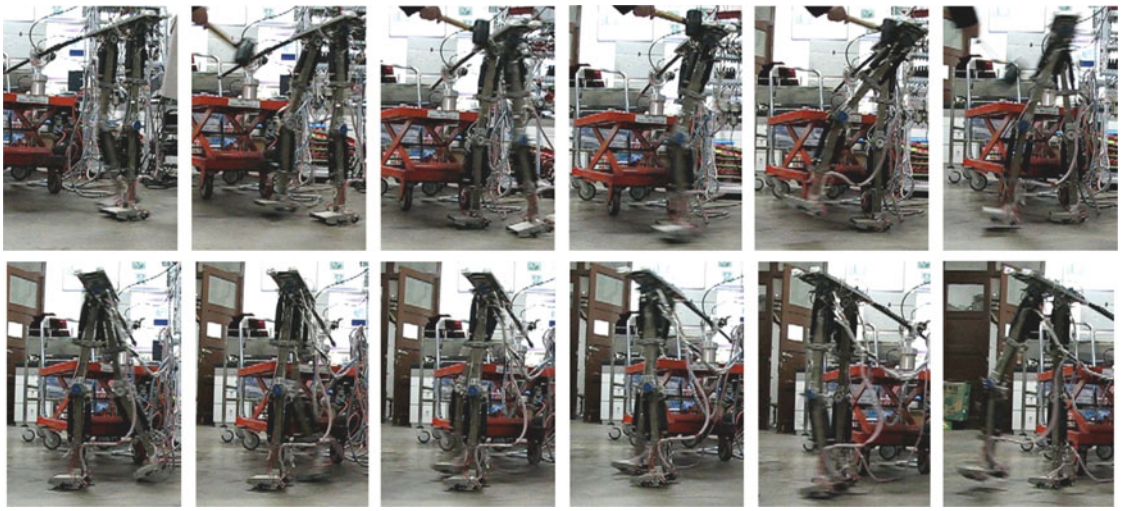


Fig. 21. Frames of walking experiment with backward disturbance.

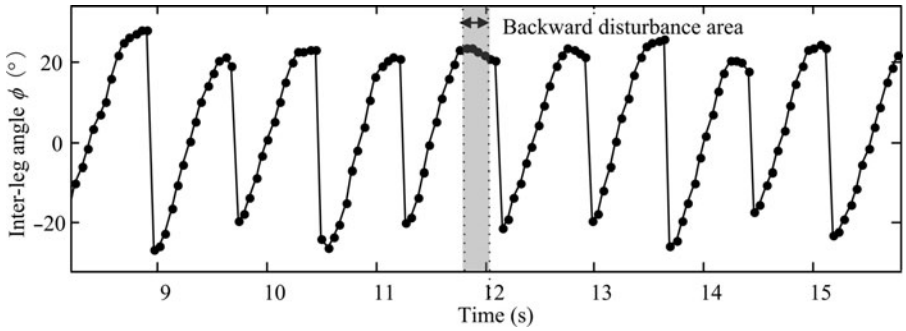


Fig. 22. Inter-leg angle versus time during walking with backward disturbance.

to evolution states and sensory feedback of biped walking. The results of this paper are summarized as follows:

1. The overall control strategy is made up of rhythm motion controller and torso attitude controller. The rhythm motion is generated by motor neurons according to a reflex network, and torso attitude controller is used to hold the torso at a desired angle.
2. We introduce global motion, leg synchronization, and joint angle as sensory feedback to activate motor neurons. The absolute angle of pendulum is utilized as a global motion feedback to realize global entrainment between the biped robot and the environment. Leg synchronization is used to coordinate the support leg with the swing leg. Joint angle feedback is designed to mimic human muscle behavior.
3. We demonstrate that the walking strategy is not only stable for a wide range of control parameters but also robust against external disturbance. Experiments have been conducted to confirm the validity of the proposed method.

Instead of tracking the predetermined trajectories, our proposed strategy generates the walking behavior through interactions between the robot dynamics, the controller, and the environment, which are crucial in control of locomotion.

The control parameters are currently selected manually from pre-calculated desired motion ranges and stability. While it has not yet been formalized to an automatic selection of these parameters with respect to specified objects, the relationships between walking indices and control parameters have been reasonably precisely described in atlases. It is possible to automatically synthesize a set of feasible parameters with respect to a given object using these atlases[29] or the iterative Newton–Raphson method. Our reflex-based approach has a small number of parameters, which may make the automatic optimization practical.

https://doi.org/10.1017/S0263574714002008 Published online by Cambridge University Press

Since proportional valves are placed outside the biped in the experiment, the air tube between the muscle and the valve is long. The length of the air tube has an effect on the speed of air muscle. This limitation leads to a short radial bar and results in the mobility of leg tip in the sagittal plane, which has an effect on walking. The robot usually takes about 10 steps (half a circle) in the experiment. Placing valves on the torso needs more powerful and longer muscle. We will consider it in the future study.

Acknowledgments

The authors would like to acknowledge financial support by the National Natural Science Foundation of China under Grant 61375099 and the reviewers for their constructive comments and suggestions.

References

1. H. Lim, Y. Yamamoto and A. Takanishi, "Control to Realize Human-Like Walking of a Biped Humanoid Robot," *Proceedings of the IEEE Conference on System, Man and Cybernetics*, Nashville, TN, USA (Oct. 2000) pp. 3271–3276.
2. C. Fu and K. Chen, "Gait synthesis and sensory control of stair climbing for a humanoid robot," *IEEE Trans. Ind. Electron.* **55**(5), 2111–2120 (2008).
3. H. Reichert, *Neurobiologie* (Thieme Georg Verlag, Stuttgart, Germany, 2000).
4. K. Matsuoka, "Sustained oscillations generated by mutually inhibiting neurons with adaption," *Biol. Cybern.* **52**(6), 367–376 (1985).
5. G. Taga, Y. Yamaguchi and H. Shimizu, "Self-organized control in bipedal locomotion by neural oscillators in unpredictable environment," *Biol. Cybern.* **65**, 147–159 (1991).
6. L. Righetti and A. J. Ijspeert, "Programmable Central Pattern Generators: An Application to Biped Locomotion Control," *Proceedings of the IEEE Conference on Robotics Automation*, Orlando, FL, USA (May 2006), pp. 1585–1590.
7. C. Fu, F. Tan and K. Chen, "A simple walking strategy for biped walking based on an intermittent sinusoidal oscillator," *Robotica* **28**(6), 869–884 (2010).
8. F. Clarac, D. Cattaert and D. L. Ray, "Central control components of a 'simple' stretch reflex," *Trends Neurosci.* **23**(5), 199–208 (2000).
9. H. Cruse and H. Warnecke, "Coordination of the legs of a slow-walking cat," *Exp. Brain Res.* **89**(1), 147–156 (1992).
10. H. Cruse, T. Kindermann and M. Schumm, "Walknet – a biologically inspired network to control six-legged walking," *Neural Netw.* **11**(7), 1435–1447 (1998).
11. R. Zaier and F. Nagashima, "Motion Pattern Generator and Reflex System for Humanoid Robots," *Proceedings of the IEEE/RSJ Conference on Intelligent Robots and Systems*, Beijing, China (Oct. 2006), pp. 840–845.
12. G. Boone and J. Hodgins, "Slipping and tripping reflexes for bipedal robots," *Auton. Robots* **4**(3), 259–271 (1997).
13. H. Funabashi, Y. Takeda, S. Itoh and M. Higuchi, "Disturbance compensating control of a biped walking machine based on reflex motions," *JSME Int. J.* **44**(3), 724–730 (2001).
14. T. Geng, B. Porr and F. Worgotter, "Fast biped walking with a sensor-driven neuronal controller and real-time online learning," *Int. J. Robot. Res.* **25**(3), 243–259 (2006).
15. P. Manoonpong, T. Geng, T. Kulvicius, B. Porr and F. Worgotter, "Adaptive, fast walking in a biped robot under neuronal control and learning," *PLos Comput. Biol.* **3**(7), 1305–1320 (2007).
16. J. W. Grizzle, G. Abba and F. Plestan, "Asymptotically stable walking for biped robots: Analysis via systems with impulse effects," *IEEE Trans. Autom. Control* **46**(1), 51–64 (2001).
17. E. R. Westervelt, G. Buche and J. W. Grizzle, "Experimental validation of a framework for the design of controllers that induce stable walking in planar bipeds," *Int. J. Robot. Res.* **23**(6), 1–24 (2004).
18. Y. Harata, F. Asano, K. Taji and Y. Uno, "Parametric excitation-based inverse bending gait generation," *Robotica* **29**(6), 831–841 (2011).
19. Y. Harata, F. Asano, Z.-W. Luo, K. Taji and Y. Uno, "Biped gait generation based on parametric excitation by knee-joint actuation," *Robotica* **27**(6), 1063–1073 (2009).
20. Y. Hurmuzlu and D. B. Marghitu, "Rigid body collisions of planar kinematic chains with multiple contact points," *Int. J. Robot. Res.* **13**(1), 82–92 (1994).
21. T. McGeer, "Passive Walking with Knees," *Proceedings of the IEEE Conference on Robotics and Automation*, Cincinnati, OH, USA (May 1990), pp. 1640–1645.
22. S. H. Collins, M. Wisse and A. Ruina, "A three-dimensional passive-dynamic walking robot with two legs and knees," *Int. J. Robot. Res.* **20**(2), 607–615 (2001).
23. R. W. Sinnet and A. D. Ames, "2D Bipedal Walking with Knees and Feet: A Hybrid Control Approach," *Proceedings of the IEEE Conference on Decision and Control*, Shanghai, China (Dec. 2009), pp. 3200–3207.
24. K. Ono, T. Furuichi and R. Takahashi, "Self-excited walking of a biped mechanism with feet," *Int. J. Robot. Res.* **23**(1), 55–68 (2004).
25. B. Thuilot, A. Goswami and B. Espiau, "Bifurcation and Chaos in a Simple Passive Bipedal Gait," *Proceedings of the IEEE Conference on Robotics Automation*, Albuquerque, NM, USA (Apr. 1997), pp. 792–798.

https://doi.org/10.1017/S0263574714002008 Published online by Cambridge University Press

26. M. Wisse, A. L. Schwab, R. Q. vd Linde and F. C. T. vd Helm, "How to keep from falling forward: Elementary swing leg action for passive dynamic walkers," *IEEE Trans. Robot.* **21**(3), 393–401 (2005).
27. T. McGeer, "Passive dynamic walking," *Int. J. Robot. Res.* **9**(2), 62–82 (1990).
28. T. Wadden and O. Ekeberg, "A neuro-mechanical model of legged locomotion: Single leg control," *Biol. Cybern.* **79**(2), 161–173 (1998).
29. C. Fu, M. Shuai, Y. Huang, J. Wang and K. Chen, "Parametric Walking Patterns and Optimum Atlases for Underactuated Biped Robots," *Proceedings of the IEEE/RSJ Conference on Intelligent Robots and Systems*, Beijing, China (Oct. 2006), pp. 342–347.

Appendix A: Motion Equations for 4-DOF Phase

$$
\begin{aligned}
D4_{11} &= m_s\left(l_s^2r_s^2+l_t^2\right)+m_h\left(l_h^2r_h^2+l_l^2\right)+m_tl_t^2r_t^2+m_ll_l^2\left(r_l^2-2r_l+2\right)-2\left(m_tr_t+m_s\right)\\
&\quad\times l_ll_t\cos(q_3-q_2)+2m_hl_ll_hr_h\cos q_2+2m_sl_tl_sr_s\cos q_4-2m_sl_ll_sr_s\cos(-q_2+q_3+q_4)\\
&\quad+I_t+I_h+I_s+I_l.\\
D4_{12} &= 2m_ll_l^2(r_l-1-r_t^2/2)-I_l-m_hl_l^2-m_hl_ll_hr_h\cos q_2+m_sl_ll_sr_s\cos(q_3+q_4-q_2)\\
&\quad+(m_tr_t+m_s)l_ll_t\cos(q_3-q_2),\\
D4_{13} &= -m_s(l_t^2+l_s^2r_s^2)-m_tl_t^2r_t^2-I_t-I_s-2m_sl_tl_sr_s\cos q_4+(m_tr_t+m_s)l_ll_t\cos(q_3-q_2)\\
&\quad+m_sl_ll_sr_s\cos(q_3+q_4-q_2),\\
D4_{14} &= -m_sl_tl_sr_s\cos q_4+m_sl_ll_sr_s\cos(q_3+q_4-q_2)-m_sl_s^2r_s^2-I_s,\\
D4_{22} &= m_ll_l^2(2-2r_l+r_l^2)+I_l+m_hl_l^2,\\
D4_{23} &= -m_sl_sl_lr_s\cos(q_3+q_4-q_2)-(m_s+m_tr_t)l_tl_l\cos(q_3-q_2),\\
D4_{24} &= -m_sl_sl_lr_s\cos(q_3+q_4-q_2),\\
D4_{33} &= I_t+I_s+m_s(l_t^2+l_s^2r_s^2)+m_tl_t^2r_t^2+2m_sl_tl_sr_s\cos q_4,\\
D4_{34} &= I_s+m_sl_s^2r_s^2+m_sl_tl_sr_s\cos q_4,\\
D4_{44} &= I_s+m_sl_s^2r_s^2,\\
C4_{11} &= (\dot q_3-\dot q_2)(m_tr_t+m_s)l_ll_t\sin(q_3-q_2)-\dot q_2m_hl_ll_hr_h\sin(q_2)+(\dot q_4+\dot q_3-\dot q_2)m_sl_ll_sr_s\\
&\quad\times\sin(q_4+q_3-q_2)-m_sl_tl_sr_s\sin(q_4)\dot q_4,\\
C4_{12} &= -l_l(\dot q_1-\dot q_2)((m_tr_t+m_s)l_t\sin(q_3-q_2)+m_sl_sr_s\sin(q_4+q_3-q_2)+m_hl_hr_h\sin q_2),\\
C4_{13} &= (\dot q_1-\dot q_3)(m_tr_t+m_s)l_ll_t\sin(q_3-q_2)+m_sl_tl_sr_s\sin(q_4)\dot q_4+(\dot q_1-\dot q_3-\dot q_4)\\
&\quad\times m_sl_ll_sr_s\sin(q_4+q_3-q_2),\\
C4_{14} &= m_sl_sr_s(l_l\sin(q_4+q_3-q_2)-l_l\sin q_4)(\dot q_1-\dot q_3-\dot q_4),\\
C4_{21} &= -l_l((\dot q_3-\dot q_1)(m_tr_t+m_s)l_t\sin(q_3-q_2)-\dot q_1m_hl_hr_h\sin q_2+(\dot q_3+\dot q_4-\dot q_1)\\
&\quad\times m_sl_sr_s\sin(q_4+q_3-q_2)),\\
C4_{23} &= l_l((\dot q_3-\dot q_1)(m_tr_t+m_s)l_t\sin(q_3-q_2)-\dot q_1m_sl_sr_s\sin(q_4+q_3-q_2)),\\
C4_{24} &= (\dot q_4+\dot q_3-\dot q_1)m_sl_ll_sr_s\sin(q_4+q_3-q_2),\\
C4_{31} &= -\dot q_1m_sl_ll_t\sin(q_3-q_2)-\dot q_1m_sl_ll_sr_s\sin(q_4+q_3-q_2)-\dot q_1m_tl_ll_tr_t\sin(q_3-q_2)\\
&\quad+\dot q_2m_tl_ll_tr_t\sin(q_3-q_2)+\dot q_2m_sl_ll_t\sin(q_3-q_2)+\dot q_2m_sl_ll_sr_s\sin(q_4+q_3-q_2)\\
&\quad+\dot q_4m_sl_tl_sr_s\sin q_4,\\
C4_{32} &= l_l(\dot q_1-\dot q_2)(m_sl_sr_s\sin(q_4+q_3-q_2)+m_sl_s\sin(q_3-q_2)+m_tl_tr_t\sin(q_3-q_2)),\\
C4_{33} &= -\dot q_4m_sl_tl_sr_s\sin q_4,
\end{aligned}
$$

https://doi.org/10.1017/S0263574714002008 Published online by Cambridge University Press

$$C4_{34} = (\dot{q}_1 - \dot{q}_3 - \dot{q}_4)m_s l_t l_s r_s \sin q_4,$$
$$C4_{41} = -m_s l_s r_s((\dot{q}_1 - \dot{q}_2)l_l \sin(q_4 + q_3 - q_2) + (\dot{q}_3 - \dot{q}_1)l_t \sin q_4,$$
$$C4_{42} = m_s l_l l_s r_s(\dot{q}_1 - \dot{q}_2)\sin(q_4 + q_3 - q_2),$$
$$C4_{43} = (\dot{q}_3 - \dot{q}_1)m_s l_t l_s r_s \sin q_4,$$
$$\begin{aligned} G4_1 = &-g(m_h l_l \sin(q_1 - q_2) + m_h l_h r_h \sin q_1 + (1 - r_l)m_l l_l \sin(q_1 - q_2) + m_t l_l \sin(q_1 - q_2) \\ &- m_t l_t r_t \sin(q_1 - q_3) + m_s l_l \sin(q_1 - q_2) - m_s l_t \sin(q_1 - q_3) - m_s l_s r_s \sin(q_1 - q_3 - q_4)), \end{aligned}$$
$$G4_2 = g l_l \sin(q_1 - q_2)(m_h + m_l - m_l r_l + m_t + m_s),$$
$$G4_3 = -g(m_t l_t r_t \sin(q_1 - q_3) + m_s l_t \sin(q_1 - q_3) + m_s l_s r_s \sin(q_1 - q_3 - q_4)),$$
$$G4_4 = -m_s g l_s r_s \sin(q_1 - q_3 - q_4).$$

Appendix B: Motion Equations for 3-DOF Phase

$$\begin{aligned} D3_{11} = &2m_l l_l^2 + I_h + m_h l_l^2 - 2m_l l_l^2 r_l \cos(q_2 - q_3) + r_h^2 l_h^2 m_h - 2m_l l_l^2 r_l + 2m_l l_l^2 r_l^2 \\ &+ 2m_h l_l l_h r_h \cos q_2 + 2I_l, \end{aligned}$$
$$D3_{12} = -m_h l_l l_h r_h \cos q_2 - I_l - m_h l_l^2 - 2m_l l_l^2 + 2m_l l_l^2 r_l - m_l l_l^2 r_l^2 + m_l l_l^2 r_l \cos(q_2 - q_3),$$
$$D3_{13} = m_l l_l^2 r_l \cos(q_2 - q_3) - I_l - m_l l_l^2 r_l^2,$$
$$D3_{22} = 2m_l l_l^2 + m_h l_l^2 + m_l l_l^2 r_l^2 - 2m_l l_l^2 r_l + I_l,$$
$$D3_{23} = -m_l l_l^2 r_l \cos(q_2 - q_3),$$
$$D3_{33} = I_l + m_l l_l^2 r_l^2,$$
$$C3_{11} = l_l(\dot{q}_2 m_l l_l r_l \sin(q_2 - q_3) - \dot{q}_2 m_h l_h r_h \sin q_2 - \dot{q}_3 m_l l_l r_l \sin(q_2 - q_3)),$$
$$C3_{12} = l_l(\dot{q}_1 - \dot{q}_2)(m_l l_l r_l \sin(q_2 - q_3) - m_h l_h r_h \sin q_2),$$
$$C3_{13} = -m_l l_l^2 r_l \sin(q_2 - q_3)(\dot{q}_1 - \dot{q}_3),$$
$$C3_{21} = -l_l(-\dot{q}_1 m_h l_h r_h \sin q_2 + \dot{q}_1 m_l l_l r_l \sin(q_2 - q_3) - \dot{q}_3 m_l l_l r_l \sin(q_2 - q_3)),$$
$$C3_{23} = (\dot{q}_1 - \dot{q}_3)m_l l_l^2 r_l \sin(q_2 - q_3),$$
$$C3_{31} = (\dot{q}_1 - \dot{q}_2)m_l l_l^2 r_l \sin(q_2 - q_3),$$
$$C3_{32} = -(\dot{q}_1 - \dot{q}_2)m_l l_l^2 r_l \sin(q_2 - q_3),$$
$$\begin{aligned} G3_1 = &-g(m_h l_l \sin(q_1 - q_2) + m_h l_h r_h \sin q_1 + 2m_l l_l \sin(q_1 - q_2) - m_l l_l r_l \sin(q_1 - q_2) \\ &- m_l l_t r_l \sin(q_1 - q_3)), \end{aligned}$$
$$G3_2 = g l_l \sin(q_1 - q_2)(m_h + 2m_l l_l - m_l r_l),$$
$$G3_3 = m_l g l_l r_l \sin(q_3 - q_1).$$

Appendix C: Motion Equations for Ground Collision Model

$$D_{f11} = D3_{11},\ D_{f12} = D3_{12},\ D_{f13} = D3_{13},\ D_{f22} = D3_{22},\ D_{f23} = D3_{23},\ D_{f33} = D3_{33},$$
$$\begin{aligned} D_{f14} = &m_h l_l \cos(q_1 - q_2) + 2m_l l_l \cos(q_1 - q_2) + m_h l_h r_h \cos q_1 - m_l l_l r_l \cos(q_1 - q_2) \\ &- m_l l_l r_l \cos(q_1 - q_3), \end{aligned}$$

https://doi.org/10.1017/S0263574714002008 Published online by Cambridge University Press

$$
\begin{aligned}
D_{\mathrm{f15}} &= m_l l_l r_l \sin(q_1 - q_2) - 2m_l l_l \sin(q_1 - q_2) - m_h l_h r_h \sin q_1 - m_h l_l \sin(q_1 - q_2) \\
&\quad + m_l l_l r_l \sin(q_1 - q_3), \\
D_{\mathrm{f24}} &= -(m_h + 2m_l - m_l r_l) l_l \cos(q_1 - q_2), \\
D_{\mathrm{f25}} &= (m_h + 2m_l - m_l r_l) l_l \sin(q_1 - q_2), \\
D_{\mathrm{f34}} &= m_l l_l r_l \cos(q_1 - q_3), \\
D_{\mathrm{f35}} &= -m_l l_l r_l \sin(q_1 - q_3), \\
D_{\mathrm{f44}} &= m_h + 2m_l, \\
D_{\mathrm{f45}} &= 0, \\
D_{\mathrm{f55}} &= m_h + 2m_l, \\
\mathbf{E}(\mathbf{q}_{\mathrm{f}}) &= \begin{bmatrix} z_x + l_l \sin(q_1 - q_2) + l_l \sin(q_3 - q_1) \\ z_y + l_l \cos(q_1 - q_2) - l_l \cos(q_3 - q_1) \end{bmatrix}.
\end{aligned}
$$

https://doi.org/10.1017/S0263574714002008 Published online by Cambridge University Press